



Published in final edited form as:

Int J Radiat Oncol Biol Phys. 2014 October 01; 90(2): 414–422. doi:10.1016/j.ijrobp.2014.06.006.

Pulmonary Ventilation Imaging based on Four-dimensional CT: Comparison with Pulmonary Function Tests and SPECT Ventilation Images

Tokihiro Yamamoto, Ph.D.^{1,2}, Sven Kabus, Ph.D.³, Cristian Lorenz, Ph.D.³, Erik Mittra, M.D., Ph.D.⁴, Julian C. Hong, M.S.¹, Melody Chung¹, Neville Eclov¹, Jacqueline To¹, Maximilian Diehn, M.D., Ph.D.¹, Billy W Loo Jr., M.D., Ph.D.¹, Paul J. Keall, Ph.D.⁵

¹Departments of Radiation Oncology, Stanford University School of Medicine, Stanford, California

²Department of Radiation Oncology, University of California Davis School of Medicine, Sacramento, California

³Department of Digital Imaging, Philips Research Europe, Hamburg, Germany

⁴Departments of Radiology, Stanford University School of Medicine, Stanford, California

⁵Sydney Medical School, University of Sydney, Sydney, New South Wales, Australia

Abstract

Purpose/Objective—Four-dimensional (4D) computed tomography (CT)-based pulmonary ventilation imaging is an emerging functional imaging modality. The purpose of this study was to investigate the physiological significance of 4D-CT ventilation imaging by comparing with pulmonary function test (PFT) measurements and single-photon emission CT (SPECT) ventilation images, which are the clinical references for global and regional lung function, respectively.

Methods and Materials—In an institutional review board-approved prospective clinical trial, 4D-CT imaging and PFT and/or SPECT ventilation imaging were performed for thoracic cancer patients. Regional ventilation (V_{4DCT}) was calculated by deformable image registration of 4D-CT images and quantitative analysis for regional volume change. V_{4DCT} defect parameters were compared with the PFT measurements (forced expiratory volume in 1 s (FEV_1) (% predicted) and FEV_1 /forced vital capacity (FVC) (%)). V_{4DCT} was also compared with SPECT ventilation (V_{SPECT}) to: (1) test whether V_{4DCT} in V_{SPECT} defect regions is significantly lower than in non-defect regions using the two-tailed t -test; (2) quantify the spatial overlap between V_{4DCT} and V_{SPECT} defect regions with the Dice similarity coefficient (DSC); and (3) test ventral-to-dorsal gradients using the two-tailed t -test.

Reprint request to: Tokihiro Yamamoto, Ph.D., Department of Radiation Oncology, University of California Davis School of Medicine, 4501 X St., Sacramento, California 95817. Tel: (916) 734-0604; toyamamoto@ucdavis.edu.

Publisher's Disclaimer: This is a PDF file of an unedited manuscript that has been accepted for publication. As a service to our customers we are providing this early version of the manuscript. The manuscript will undergo copyediting, typesetting, and review of the resulting proof before it is published in its final citable form. Please note that during the production process errors may be discovered which could affect the content, and all legal disclaimers that apply to the journal pertain.

Conflict of interest: Dr. Yamamoto receives non-financial support from Philips Radiation Oncology Systems. Dr. Kabus and Dr. Lorenz are employees of Philips Research. Dr. Keall has a patent, Method and system for using computed tomography to test pulmonary function (US 7668357) issued.

Results—Out of 21 patients enrolled onto the study, 18 patients, for which 4D-CT and either PFT or SPECT was acquired, were included in the analysis. V_{4DCT} defect parameters were found to have significant, moderate correlations with the PFT measurements. For example, V_{4DCT}^{HU} defect volume increased significantly with decreasing FEV_1/FVC ($R=-0.65$, $p<0.01$). V_{4DCT} in V_{SPECT} defect regions was significantly lower than in non-defect regions (mean V_{4DCT}^{HU} 0.049 vs. 0.076, $p<0.01$). The average DSCs for the spatial overlap with SPECT ventilation defect regions were only moderate (V_{4DCT}^{HU} 0.39±0.11). Furthermore, ventral-to-dorsal gradients of V_{4DCT} were strong (V_{4DCT}^{HU} $R^2=0.69$, $p=0.08$), which was similar to V_{SPECT} ($R^2=0.96$, $p<0.01$).

Conclusions—An 18-patient study demonstrated significant correlations between 4D-CT ventilation and PFT measurements as well as SPECT ventilation, providing evidence towards the validation of 4D-CT ventilation imaging.

Introduction

Despite technological advances in the field, overall survival for lung cancer remains disappointing and toxicity is substantial. Radiation pneumonitis is a common, potentially fatal toxicity that occurs in up to 30% of lung cancer patients treated with radiotherapy [1–3]. Radiotherapy that selectively avoids irradiating highly-functional lung regions may reduce pulmonary toxicity. This hypothesis is supported by several reports in the literature demonstrating that pulmonary toxicity correlates more strongly with the functional dose-volume parameters than the anatomic parameters (current clinical standard) [4–6]. For example, Vinogradskiy *et al.* found that the functional (ventilation) parameters (*e.g.*, functional mean lung dose) had stronger correlations with Grade 3 pneumonitis than the anatomic parameters (*e.g.*, mean lung dose) for 96 non-small-cell lung cancer (NSCLC) patients [6].

There have been many modalities for pulmonary ventilation imaging, including single-photon emission computed tomography (SPECT) [7], positron emission tomography (PET) [8], magnetic resonance (MR) [9–11], and dual-energy CT [12]. Ventilation images can also be acquired by an emerging technique based on four-dimensional (4D) or biphasic (exhalation and inhalation) CT, deformable image registration (DIR) and quantitative analysis [13–15]. Compared to other modalities, 4D-CT ventilation imaging has a higher resolution (the exact spatial resolution is unknown), lower cost, shorter scan time, and/or greater availability. 4D-CT ventilation can be considered ‘free’ information for lung cancer patients treated with radiotherapy [14,16], as 4D-CT scans are currently in routine use for radiotherapy at most centers [17] and ventilation computation involves only image processing and analysis. Prior to clinical applications, 4D-CT ventilation imaging should be validated against ground truth. Animal studies have demonstrated strong correlations between 4D-CT ventilation and xenon CT ventilation [15,18], and also high reproducibility [19]. However, human studies have reported inconsistent results [19–22], *e.g.*, reasonable correlations with hyperpolarized ^3He MR ventilation [21], whereas weak correlations with ^{99m}Tc -labeled diethylenetriamine pentaacetate (DTPA) SPECT ventilation [20]. Also only poor to moderate reproducibility has been demonstrated [19,22]. These results suggest the need for further validation. The purpose of this study was to investigate the physiological

significance of 4D-CT ventilation imaging by comparing with: (1) PFT measurements as the clinical reference for global lung function, and (2) ^{99m}Tc -DTPA SPECT ventilation as the clinical reference for regional ventilation, for patients with thoracic cancer.

Methods and Materials

Study Design

This study was a prospective, single-arm, single-institutional clinical trial approved by the institutional review board. All patients provided written informed consent. Patients were eligible for participation if they had a primary or metastatic thoracic cancer to be treated with radiotherapy, and were 18 years of age. We performed 4D-CT imaging (standard of care) as well as PFT and/or SPECT ventilation imaging with an attempt to acquire all the data prior to treatment (Figure e1).

4D-CT Ventilation Imaging

The first step of 4D-CT ventilation imaging was 4D-CT scans acquired in the supine posture on a Discovery ST multislice PET/CT scanner (GE Healthcare, Waukesha, WI). Scan parameters were: 120 kVp, approximately 100 mAs per slice, 0.5 s gantry rotation, 0.45 s cine interval, and 2.5 mm slice thickness. The CT data segments were then sorted into ten respiratory bins by the phase-based method using GE Advantage 4D software and anatomic similarity-based method designed to reduce artifacts [23]. The resulting 4D-CT image with fewer 4D-CT artifacts was identified qualitatively and quantitatively using the normalized cross correlation-based artifact score [24], and was selected for ventilation computation and the subsequent analysis.

The second step was DIR for spatial mapping of the peak-inhale 4D-CT image (moving) to the peak-exhale image (fixed). We used a volumetric elastic DIR method that minimizes both a similarity function (sum of squared difference between the peak-exhale and deformed peak-inhale 4D-CT images) and a regularizing term (elastic regularizer) based on the Navier-Lamé equation. Further details of the algorithm have been described elsewhere [25]. The registration accuracy was previously studied by quantifying the target registration error for anatomic landmarks in the lung, which were found to be less than the voxel dimension on average [25–27]. The algorithm was evaluated in the MICCAI EMPIRE10 challenge and placed Xth among 34 participants [27]. Note that the accuracy for the cohort of patients used in this study has not been evaluated.

The final step was to quantify regional volume change per lung voxel volume, yielding a 4D-CT ventilation image at the peak-exhale phase ($V_{4\text{DCT}}$). We investigated two different metrics: Hounsfield unit (HU) change-based ($V_{4\text{DCT}}^{\text{HU}}$) and Jacobian-based ($V_{4\text{DCT}}^{\text{Jac}}$). $V_{4\text{DCT}}^{\text{HU}}$ was defined based on the relationship between the regional HU change and regional volume change [13,28] as well as CT density scaling, expressed as

$$V_{4\text{DCT}}^{\text{HU}}(x, y, z) = \frac{\text{HU}_{\text{ex}}(x, y, z) - \text{HU}_{\text{in}}\{x + u_x(x, y, z), y + u_y(x, y, z), z + u_z(x, y, z)\}}{\text{HU}_{\text{in}}\{x + u_x(x, y, z), y + u_y(x, y, z), z + u_z(x, y, z)\} + 1000} \rho_{\text{scaling}}$$

where HU is the HU value, u is the displacement vector mapping the voxel at location (x, y, z) of a peak-exhale image to the corresponding location of a peak-inhale image, and ρ_{scaling} is the CT density scaling factor, $\rho_{\text{scaling}} = (\text{HU}_{\text{ex}} + 1024)/774$, which takes a value ranging from 0 for the voxel with the lowest lung CT density (-1024 HU) to 1 for the voxel with the highest density (-250 HU), in a similar manner to Kipritidis *et al.* [29]. The rationale for density scaling is to transform a purely mechanical model of regional ventilation based on volume change alone to a more physiological model. Gas transport to high alveolar density regions contributes more to gas exchange, and hence is considered more physiologically relevant compared to gas transport to low alveolar density regions. It was assumed that alveolar density was proportional to CT density. In the same manner as Guerrero *et al.* [14], mass correction was applied to HU_{in} to account for the difference in the lung mass between the peak-exhale and peak-inhale phases. $V_{4\text{DCT}}^{\text{Jac}}$ was defined by

$$V_{4\text{DCT}}^{\text{Jac}}(x, y, z) = \left(\begin{array}{ccc|c} 1 + \frac{\partial u_x(x, y, z)}{\partial x} & \frac{\partial u_x(x, y, z)}{\partial y} & \frac{\partial u_x(x, y, z)}{\partial z} & \\ \frac{\partial u_y(x, y, z)}{\partial x} & 1 + \frac{\partial u_y(x, y, z)}{\partial y} & \frac{\partial u_y(x, y, z)}{\partial z} & \\ \frac{\partial u_z(x, y, z)}{\partial x} & \frac{\partial u_z(x, y, z)}{\partial y} & 1 + \frac{\partial u_z(x, y, z)}{\partial z} & \\ \hline & & & -1 \end{array} \right) \rho_{\text{scaling}}.$$

The detailed derivation of the equations for $V_{4\text{DCT}}^{\text{HU}}$ and $V_{4\text{DCT}}^{\text{Jac}}$ is described in Appendix e1. For both $V_{4\text{DCT}}^{\text{HU}}$ and $V_{4\text{DCT}}^{\text{Jac}}$, a value <0 indicates regional contraction and a value >0 indicates regional expansion. The lung parenchyma was segmented by delineating lung voxels with -250 HU [14] within the lung outlines generated by the model-based segmentation of a Pinnacle³ radiotherapy treatment planning system (Philips Radiation Oncology Systems, Fitchburg, WI).

Comparison of 4D-CT Ventilation Defect Parameters with Pulmonary Function Test (PFT) Measurements

PFT was performed to measure forced expiratory volume in 1 s (FEV_1) (% predicted), forced vital capacity (FVC) (% predicted), FEV_1/FVC (%), and diffusing capacity of the lung for carbon monoxide (DL_{CO}) (% predicted) with a HDpft system (nSpire Health, Longmont, CO) according to American Thoracic Society (ATS)/European Respiratory Society (ERS) guidelines [30]. FEV_1 and FEV_1/FVC were chosen to analyze the Pearson correlation with $V_{4\text{DCT}}$ defect parameters, given that these parameters have been found to correlate significantly with hyperpolarized gas MR ventilation defect parameters [31,32]. We investigated the following $V_{4\text{DCT}}$ defect parameters: (1) the lowest 25th percentile $V_{4\text{DCT}}$ value, (2) absolute defect volume (1), and (3) % defect volume. Given that no data is available on 4D-CT ventilation threshold values to identify defect regions, the threshold was determined by finding a value which gives the average % defect volume of approximately 25%. Mathew *et al.* found the average % defect volume of 25% for a similar cohort of patients with hyperpolarized ³He MR ventilation imaging [21,33]. The threshold was found to be 0.015, yielding the mean volume of 1.1 ± 1.4 l ($25 \pm 21\%$ of the total lung volume) for $V_{4\text{DCT}}^{\text{HU}}$ and 1.2 ± 1.5 l ($25 \pm 20\%$) for $V_{4\text{DCT}}^{\text{Jac}}$.

Comparison of 4D-CT Ventilation with SPECT Ventilation

V_{4DCT} was compared with V_{SPECT} to: (1) test whether V_{4DCT} in V_{SPECT} defect regions is significantly lower than in non-defect regions; (2) quantify the spatial overlap between V_{4DCT} and V_{SPECT} defect regions; and (3) test ventral-to-dorsal gradients. V_{SPECT} scans and low-dose CT scans for attenuation correction were acquired in the supine posture on a GE Infinia Hawkeye SPECT/CT scanner. ^{99m}Tc -DTPA was aerosolized using an Insta/Vent system (Medi/Nuclear, Baldwin Park, CA) and was then administered to the patient in the supine posture through slow, moderately deep breathing. SPECT projections were acquired in a 64×64 matrix with a 8.8×8.8 mm² pixel size, 8.8 mm slice spacing, 60 projections over 360°, and 30 s per projection during tidal breathing. SPECT images were reconstructed using the 3D ordered-subsets expectation maximization (OSEM) algorithm [34] with attenuation correction.

The low-dose CT image of SPECT was rigidly aligned with the peak-exhale 4D-CT image using the Pinnacle³ system. Central airways (plus a 1 cm margin) which were manually delineated using the Pinnacle³ system were excluded from all the comparisons of V_{4DCT} and V_{SPECT} , considering central airway depositions of ^{99m}Tc -DTPA aerosols observed frequently in patients with COPD [7].

V_{SPECT} defect regions were segmented by delineating lung voxels with a value less than a threshold, which was determined as the mean intensity of the background noise plus twice the standard deviation of the distribution of the background noise in a similar manner to Kauczor *et al.* [35], yielding the mean volume of $24 \pm 11\%$ of the total lung volume. V_{4DCT} defect regions were segmented by the method described earlier. The two-tailed *t*-test was used to examine whether V_{4DCT} in V_{SPECT} defect regions is significantly lower than in non-defect regions ($p < 0.05$). The Dice similarity coefficient (DSC) [36] was used to quantify the spatial overlap between V_{4DCT} and V_{SPECT} defect regions. Furthermore, ventral-to-dorsal gradient was evaluated to test whether 4D-CT ventilation imaging shows the known effect of gravity on ventilation, *i.e.*, greater ventilation in the dorsal region than in the ventral region due to the lung parenchyma tissue shift toward gravity dependent region. This effect has been demonstrated with other imaging modalities [11,37,38]. We quantified the slope (regression coefficient) from linear regression for the relationship between the relative ventral-to-dorsal distance and globally normalized ventilation value at the corresponding distance. The total lung was divided into five coronal section-wise regions of interest equally spaced along the ventral-to-dorsal direction. The mean ventilation value was quantified for each region of interest. Statistical analysis was performed to test whether the slope is significantly different from zero ($p < 0.05$) using the two-tailed *t*-test.

Results

Patients

Between January 2010 and December 2012, 21 patients met the eligibility criteria and were enrolled onto the study. Out of 21 patients, 4D-CT images were acquired as standard of care for all patients. FEV₁, FEV₁/FVC and SPECT data were acquired for 16, 15 and 16 patients, respectively. The data of the other patients were not available because of withdrawal from

the clinical trial or incorrect data acquisition. Eighteen patients, for whom PFT and/or SPECT data was available, were included in the analysis. Several patients received repeat 4D-CT scans and the one acquired closest to the SPECT scan time was selected for the analysis. Compared to 4D-CT, the average interval was 56 ± 53 days and the difference in the dose delivered prior to the measurement was 1 ± 3 Gy for PFT; 9 ± 10 days and 4 ± 13 Gy for SPECT. Variable intervals and the dose differences were mainly due to logistical reasons, such as patient availability, machine availability, and patient no-show.

4D-CT Ventilation Defect Parameters vs. PFT Measurements

Figure 1 shows the relationship between FEV_1/FVC and V_{4DCT}^{HU} defect parameters for 15 patients. FEV_1/FVC decreased significantly with decreasing lowest 25th percentile V_{4DCT}^{HU} value ($R=0.73$, $p<0.01$), and with increasing defect volume ($R=-0.65$, $p<0.01$) and % defect volume ($R=-0.63$, $p=0.01$). Table 2 shows correlations between V_{4DCT} defect parameters and PFT measurements. In general, both V_{4DCT}^{HU} and V_{4DCT}^{Jac} demonstrated significant, moderate correlations with FEV_1 and FEV_1/FVC , indicating that severe V_{4DCT} defect is correlated with impaired global lung function. V_{4DCT}^{Jac} had slightly stronger correlations, especially with FEV_1 , compared to V_{4DCT}^{HU} .

4D-CT Ventilation vs. SPECT Ventilation

Figure 2a shows a comparison of V_{4DCT}^{HU} and V_{SPECT} for patient 16, showing a good correlation and large separation between the probability density functions of V_{4DCT}^{HU} in V_{SPECT} defect regions and non-defect regions. The mean V_{4DCT}^{HU} value in V_{SPECT} non-defect regions (0.06 ± 0.06) was higher than in defect regions (0.02 ± 0.04), showing a clear separation between the peaks of the two probability density functions. The DSC for V_{4DCT}^{HU} and V_{SPECT} defect regions was 0.46. In contrast, patient 18 showed a poor correlation and small separation between the probability density functions of V_{4DCT}^{HU} in V_{SPECT} defect regions and non-defect regions (Figure 2b). The mean V_{4DCT}^{HU} value in V_{SPECT} non-defect regions (0.11 ± 0.08) was only slightly higher than in defect regions (0.09 ± 0.08). The DSC was 0.35. Note high V_{SPECT} values along the border between the left lung and mediastinum due to image registration errors, resulting in erroneous defect regions along the left chest wall. Both patients 16 and 18 showed non-severe central airway depositions in V_{SPECT} . V_{4DCT} values in V_{SPECT} defect regions and non-defect regions for 16 patients are summarized in Table 3. Both V_{4DCT}^{HU} and V_{4DCT}^{Jac} demonstrated significantly higher values in non-defect regions than in defect regions, whether or not 6 patients with severe central airway depositions in V_{SPECT} were excluded from the analysis. The average DSCs for the spatial overlap with V_{SPECT} regions were found to be only moderate (0.39 ± 0.11 for V_{4DCT}^{HU} ; 0.36 ± 0.13 for V_{4DCT}^{Jac}).

Figure 3 shows ventral-to-dorsal gradients of V_{4DCT} and V_{SPECT} for 16 patients. Both V_{4DCT}^{HU} and V_{4DCT}^{Jac} demonstrated strong, but statistically non-significant ventral-to-dorsal

gradients ($V_{4DCT}^{HU} R^2=0.69, p=0.08$; $V_{4DCT}^{Jac} R^2=0.68, p=0.09$), indicating higher ventilation in dorsal regions than in ventral regions. V_{SPECT} showed a strong, significant gradient ($R^2=0.96, p<0.01$). For 6 patients with severe central airway depositions in V_{SPECT} , the ventral-to-dorsal gradient was still strong, but statistically non-significant ($R^2=0.74, p=0.06$).

Discussion

This study demonstrated significant, moderate correlations between V_{4DCT} defect parameters and PFT measurements (FEV_1 and FEV_1/FVC), significantly lower V_{4DCT} in V_{SPECT} defect regions than in non-defect regions, moderate DSCs between V_{4DCT} and V_{SPECT} defect regions, and moreover strong ventral-to-dorsal gradients. These results provide evidence towards the validation of 4D-CT ventilation imaging. PFT and SPECT ventilation imaging are widely accepted clinical standard methods for the evaluation of global and regional lung function, respectively. This is the first investigation to compare 4D-CT ventilation imaging with PFT in a cohort of thoracic cancer patients. Murphy *et al.* compared biphasic (end-expiration and end-inspiration) breath-hold CT-based ventilation with PFT measurements for 126 COPD patients and found strong correlations (0.73–0.88) [39]. There are several major differences from our study, including CT image quality, breathing maneuver and patient characteristics, which might have led to stronger correlations compared to our study. Other modalities including hyperpolarized gas MR [32,33,40] were found to correlate significantly with PFT. Stavngaard *et al.* reported the correlation of 0.5 ($p<0.05$) between FEV_1 and ^{81m}Kr SPECT ventilated volume [41], which was similar to our study (FEV_1 vs. V_{SPECT} defect volume $R=-0.54, p=0.04$). Several investigators compared 4D-CT ventilation imaging with other modalities, including ^{99m}Tc -DTPA SPECT ventilation [20] and hyperpolarized 3He MR ventilation [21] for lung cancer patients. Reasonable overlaps of defect regions were observed for MR ventilation [21]. Overall only poor overlaps of percentile lung regions were reported for SPECT ventilation, whereas the overlap was relatively better in poorly-ventilated regions than in well-ventilated regions [20]. We found moderate DSCs between V_{4DCT} and V_{SPECT} defect regions, which were consistent with Castillo *et al.* [20]. Only moderate DSCs may be, at least in part, the result of spatial resolution difference. High resolution 4D-CT ventilation images provide more details and detect smaller defect regions compared to low resolution SPECT ventilation images. V_{4DCT} demonstrated significantly higher values in V_{SPECT} non-defect regions than in defect regions. However, it is unknown whether or not clinically significant. Proving a clinical significance would ultimately require clinical trials to test a clinically-relevant hypothesis.

There are several limitations in this study, including 4D-CT artifacts and limited quality of SPECT ventilation images. The current clinical standard 4D-CT technique with phase-based sorting often results in artifacts [42]. In this study, we used phase-based sorting and anatomic similarity-based sorting to use the image with fewer artifacts for the analysis, though there were residual artifacts. Recently Yamamoto *et al.* demonstrated that 4D-CT artifacts are an important source of variations in 4D-CT ventilation imaging [24]. Future developments of strategies to improve 4D-CT may increase the correlation with PFT and SPECT ventilation. Even though ^{99m}Tc -DTPA SPECT ventilation imaging is a widely

accepted clinical standard method for evaluating regional lung function, it provides images of limited quality due to low resolution and central airway depositions observed frequently in patients with COPD [7]. Considering these limitations, SPECT ventilation imaging does not necessarily provide a ground truth. For future studies, comparisons with high-quality ventilation images such as xenon CT with dual-energy CT [12,43] may provide a better understanding on the physiological significance of 4D-CT ventilation imaging.

There are several major differences between 4D-CT and PFT or SPECT, including the time, dose delivered prior to the measurement, breathing maneuver, and posture. All the measurements should ideally be acquired on the same day to minimize possible effects of time and dose differences on lung function. We consider that such effects on the results of this study would be limited for the following reasons. A subgroup analysis by dividing the patients by the median interval into two groups did not result in significant differences in the results between the two groups (data not shown). Recently Yuan *et al.* observed non-significant PFT changes during a course of treatment (at approximately 45 Gy) for 56 Stage I–III NSCLC patients who received 60 Gy, while they observed a significant improvement in SPECT ventilation [44]. Given that the dose difference in our patient cohort (PFT 1 ± 3 Gy; SPECT 4 ± 13 Gy) was considerably smaller than 45 Gy [44], the effect of dose difference on global and regional lung function is assumed to be minimal. Tumor growth over the interval period between the measurements (56 ± 53 days for PFT; 9 ± 10 days for SPECT) might affect lung function. A long interval between 4D-CT and PFT was due to the fact that several patients received PFT as part of the standard of care rather than specifically for the study. However, the effect is considered small because the intervals are well shorter than the tumor volume doubling time of 139 days (median) reported by Wang *et al.* [45]. SPECT provides respiration-averaged ventilation images, which may be better compared with 4D-CT ventilation images averaged over a respiratory cycle. Differences in positioning (*e.g.*, arm position, immobilization) between the 4D-CT and SPECT scans affected the quality of image registration. DIR algorithms optimized and validated to allow accurate registration to low-dose CT images of SPECT may increase the correlations. Given these limitations, the correlations between 4D-CT ventilation and PFT or SPECT ventilation found in this study would represent lower bounds to the true correlation.

Conclusions

An 18-patient study demonstrated significant correlations between 4D-CT ventilation images and PFT as well as SPECT ventilation images, providing evidence towards the validation of 4D-CT ventilation imaging. Further studies are needed to explore the physiological and clinical significance of 4D-CT ventilation imaging.

Supplementary Material

Refer to Web version on PubMed Central for supplementary material.

Acknowledgments

Michael Goris, M.D., Ph.D. and Lindee Burton in the Department of Radiology at Stanford provided support for the clinical trial. Eric Johnston in the Department of Electrical Engineering at Stanford assisted with 4D-CT sorting.

Lihong Qi, Ph.D. in the Department of Public Health Sciences at the University of California Davis provided advice on estimating the statistical power of the analysis. Philips Radiation Oncology Systems loaned us Pinnacle³ treatment planning systems.

Funding: This study was supported in part by National Lung Cancer Partnership Young Investigator Research Grant and NIH/NCI R01 CA 093626.

References

1. Mehta V. Radiation pneumonitis and pulmonary fibrosis in non-small-cell lung cancer: pulmonary function, prediction, and prevention. *Int J Radiat Oncol Biol Phys.* 2005; 63:5–24. [PubMed: 15963660]
2. Marks LB, Bentzen SM, Deasy JO, et al. Radiation dose-volume effects in the lung. *Int J Radiat Oncol Biol Phys.* 2010; 76:S70–76. [PubMed: 20171521]
3. Palma DA, Senan S, Tsujino K, et al. Predicting radiation pneumonitis after chemoradiation therapy for lung cancer: an international individual patient data meta-analysis. *Int J Radiat Oncol Biol Phys.* 2013; 85:444–450. [PubMed: 22682812]
4. Abratt RP, Willcox PA, Smith JA. Lung cancer in patients with borderline lung functions—zonal lung perfusion scans at presentation and lung function after high dose irradiation. *Radiother Oncol.* 1990; 19:317–322. [PubMed: 2284442]
5. Seppenwoolde Y, De Jaeger K, Boersma LJ, et al. Regional differences in lung radiosensitivity after radiotherapy for non-small-cell lung cancer. *Int J Radiat Oncol Biol Phys.* 2004; 60:748–758. [PubMed: 15465191]
6. Vinogradskiy Y, Castillo R, Castillo E, et al. Use of 4-dimensional computed tomography-based ventilation imaging to correlate lung dose and function with clinical outcomes. *Int J Radiat Oncol Biol Phys.* 2013; 86:366–371. [PubMed: 23474113]
7. Petersson J, Sanchez-Crespo A, Larsson SA, et al. Physiological imaging of the lung: single-photon-emission computed tomography (SPECT). *J Appl Physiol.* 2007; 102:468–476. [PubMed: 16990505]
8. Harris RS, Schuster DP. Visualizing lung function with positron emission tomography. *J Appl Physiol.* 2007; 102:448–458. [PubMed: 17038490]
9. Edelman RR, Hatabu H, Tadamura E, et al. Noninvasive assessment of regional ventilation in the human lung using oxygen-enhanced magnetic resonance imaging. *Nat Med.* 1996; 2:1236–1239. [PubMed: 8898751]
10. van Beek EJ, Wild JM, Kauczor HU, et al. Functional MRI of the lung using hyperpolarized 3-helium gas. *J Magn Reson Imaging.* 2004; 20:540–554. [PubMed: 15390146]
11. Bauman G, Lutzen U, Ullrich M, et al. Pulmonary functional imaging: qualitative comparison of Fourier decomposition MR imaging with SPECT/CT in porcine lung. *Radiology.* 2011; 260:551–559. [PubMed: 21586678]
12. Chae EJ, Seo JB, Goo HW, et al. Xenon ventilation CT with a dual-energy technique of dual-source CT: initial experience. *Radiology.* 2008; 248:615–624. [PubMed: 18641254]
13. Guerrero T, Sanders K, Noyola-Martinez J, et al. Quantification of regional ventilation from treatment planning CT. *Int J Radiat Oncol Biol Phys.* 2005; 62:630–634. [PubMed: 15936537]
14. Guerrero T, Sanders K, Castillo E, et al. Dynamic ventilation imaging from four-dimensional computed tomography. *Phys Med Biol.* 2006; 51:777–791. [PubMed: 16467578]
15. Reinhardt JM, Ding K, Cao K, et al. Registration-based estimates of local lung tissue expansion compared to xenon CT measures of specific ventilation. *Med Image Anal.* 2008; 12:752–763. [PubMed: 18501665]
16. Yamamoto T, Kabus S, von Berg J, et al. Impact of four-dimensional computed tomography pulmonary ventilation imaging-based functional avoidance for lung cancer radiotherapy. *Int J Radiat Oncol Biol Phys.* 2011; 79:279–288. [PubMed: 20646852]
17. Simpson DR, Lawson JD, Nath SK, et al. Utilization of advanced imaging technologies for target delineation in radiation oncology. *J Am Coll Radiol.* 2009; 6:876–883. [PubMed: 19945044]
18. Fuld MK, Easley RB, Saba OI, et al. CT-measured regional specific volume change reflects regional ventilation in supine sheep. *J Appl Physiol.* 2008; 104:1177–1184. [PubMed: 18258804]

19. Du K, Bayouth JE, Cao K, et al. Reproducibility of registration-based measures of lung tissue expansion. *Med Phys.* 2012; 39:1595–1608. [PubMed: 22380392]
20. Castillo R, Castillo E, Martinez J, et al. Ventilation from four-dimensional computed tomography: density versus Jacobian methods. *Phys Med Biol.* 2010; 55:4661–4685. [PubMed: 20671351]
21. Mathew L, Wheatley A, Castillo R, et al. Hyperpolarized (3)He magnetic resonance imaging: comparison with four-dimensional x-ray computed tomography imaging in lung cancer. *Acad Radiol.* 2012; 19:1546–1553. [PubMed: 22999648]
22. Yamamoto T, Kabus S, von Berg J, et al. Reproducibility of four-dimensional computed tomography-based lung ventilation imaging. *Acad Radiol.* 2012; 19:1554–1565. [PubMed: 22975070]
23. Johnston E, Diehn M, Murphy JD, et al. Reducing 4D CT artifacts using optimized sorting based on anatomic similarity. *Med Phys.* 2011; 38:2424–2429. [PubMed: 21776777]
24. Yamamoto T, Kabus S, Lorenz C, et al. 4D CT lung ventilation images are affected by the 4D CT sorting method. *Med Phys.* 2013; 40:101907. [PubMed: 24089909]
25. Detail omitted for blind review.
26. Detail omitted for blind review.
27. Murphy K, van Ginneken B, Reinhardt JM, et al. Evaluation of registration methods on thoracic CT: the EMPIRE10 challenge. *IEEE Trans Med Imaging.* 2011; 30:1901–1920. [PubMed: 21632295]
28. Simon BA. Non-invasive imaging of regional lung function using x-ray computed tomography. *J Clin Monit Comput.* 2000; 16:433–442. [PubMed: 12580227]
29. Kipritidis J, Siva S, Hofman MS, et al. Validating and improving CT ventilation imaging by correlating with ventilation 4D-PET/CT using (68)Ga-labeled nanoparticles. *Med Phys.* 2014; 41:011910. [PubMed: 24387518]
30. Miller MR, Hankinson J, Brusasco V, et al. Standardisation of spirometry. *Eur Respir J.* 2005; 26:319–338. [PubMed: 16055882]
31. de Lange EE, Altes TA, Patrie JT, et al. Evaluation of asthma with hyperpolarized helium-3 MRI: correlation with clinical severity and spirometry. *Chest.* 2006; 130:1055–1062. [PubMed: 17035438]
32. Kirby M, Svenningsen S, Owrangi A, et al. Hyperpolarized 3He and 129Xe MR imaging in healthy volunteers and patients with chronic obstructive pulmonary disease. *Radiology.* 2012; 265:600–610. [PubMed: 22952383]
33. Mathew L, Gaede S, Wheatley A, et al. Detection of longitudinal lung structural and functional changes after diagnosis of radiation-induced lung injury using hyperpolarized 3He magnetic resonance imaging. *Med Phys.* 2010; 37:22–31. [PubMed: 20175462]
34. Hudson HM, Larkin RS. Accelerated image reconstruction using ordered subsets of projection data. *IEEE Trans Med Imaging.* 1994; 13:601–609. [PubMed: 18218538]
35. Kauczor HU, Markstaller K, Puderbach M, et al. Volumetry of ventilated airspaces by 3He MRI: preliminary results. *Invest Radiol.* 2001; 36:110–114. [PubMed: 11224759]
36. Dice LR. Measures of the amount of ecologic association between species. *Ecology.* 1945; 26:297–302.
37. Petersson J, Rohdin M, Sanchez-Crespo A, et al. Posture primarily affects lung tissue distribution with minor effect on blood flow and ventilation. *Respir Physiol Neurobiol.* 2007; 156:293–303. [PubMed: 17169620]
38. Henderson AC, Sa RC, Theilmann RJ, et al. The gravitational distribution of ventilation-perfusion ratio is more uniform in prone than supine posture in the normal human lung. *J Appl Physiol.* 2013; 115:313–324. [PubMed: 23620488]
39. Murphy K, Pluim JP, van Rikxoort EM, et al. Toward automatic regional analysis of pulmonary function using inspiration and expiration thoracic CT. *Med Phys.* 2012; 39:1650–1662. [PubMed: 22380397]
40. Fain SB, Gonzalez-Fernandez G, Peterson ET, et al. Evaluation of structure-function relationships in asthma using multidetector CT and hyperpolarized He-3 MRI. *Acad Radiol.* 2008; 15:753–762. [PubMed: 18486011]

41. Stavngaard T, Sogaard LV, Mortensen J, et al. Hyperpolarized ^3He MRI and ^{81}mKr SPECT in chronic obstructive pulmonary disease. *Eur J Nucl Med Mol Imaging*. 2005; 32:448–457. [PubMed: 15821964]
42. Yamamoto T, Langner U, Loo BW Jr, et al. Retrospective analysis of artifacts in four-dimensional CT images of 50 abdominal and thoracic radiotherapy patients. *Int J Radiat Oncol Biol Phys*. 2008; 72:1250–1258. [PubMed: 18823717]
43. Honda N, Osada H, Watanabe W, et al. Imaging of Ventilation with Dual-Energy CT during Breath Hold after Single Vital-Capacity Inspiration of Stable Xenon. *Radiology*. 2012; 262:262–268. [PubMed: 22025733]
44. Yuan ST, Frey KA, Gross MD, et al. Changes in global function and regional ventilation and perfusion on SPECT during the course of radiotherapy in patients with non-small-cell lung cancer. *Int J Radiat Oncol Biol Phys*. 2012; 82:e631–638. [PubMed: 22197235]
45. Wang J, Mahasittiwat P, Wong KK, et al. Natural growth and disease progression of non-small cell lung cancer evaluated with ^{18}F -fluorodeoxyglucose PET/CT. *Lung Cancer*. 2012; 78:51–56. [PubMed: 22841591]

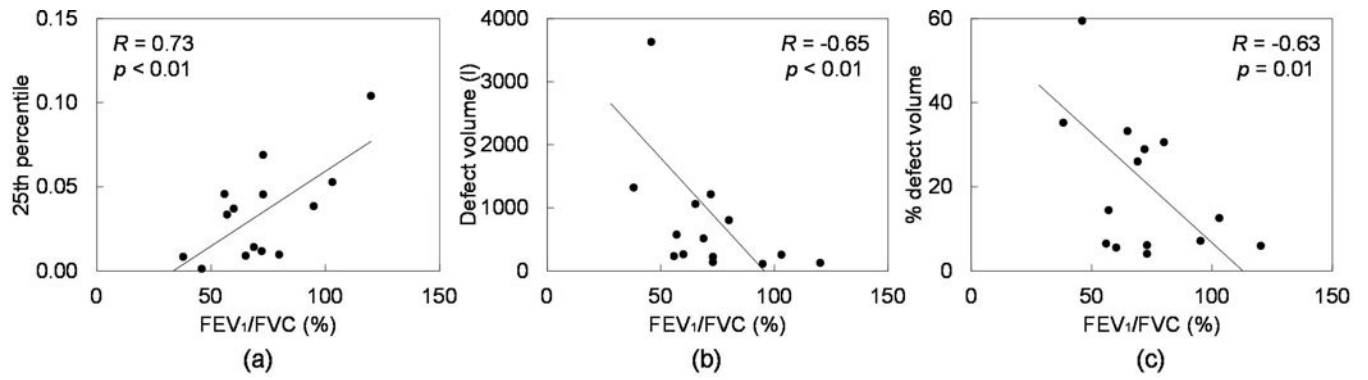


Figure 1.

FEV₁/FVC (%) vs. V_{4DCT}^{HU} defect parameters: (a) 25th percentile value, (b) absolute defect volume (l), and (c) % defect volume for 15 patients. The lines of best fit are also shown.

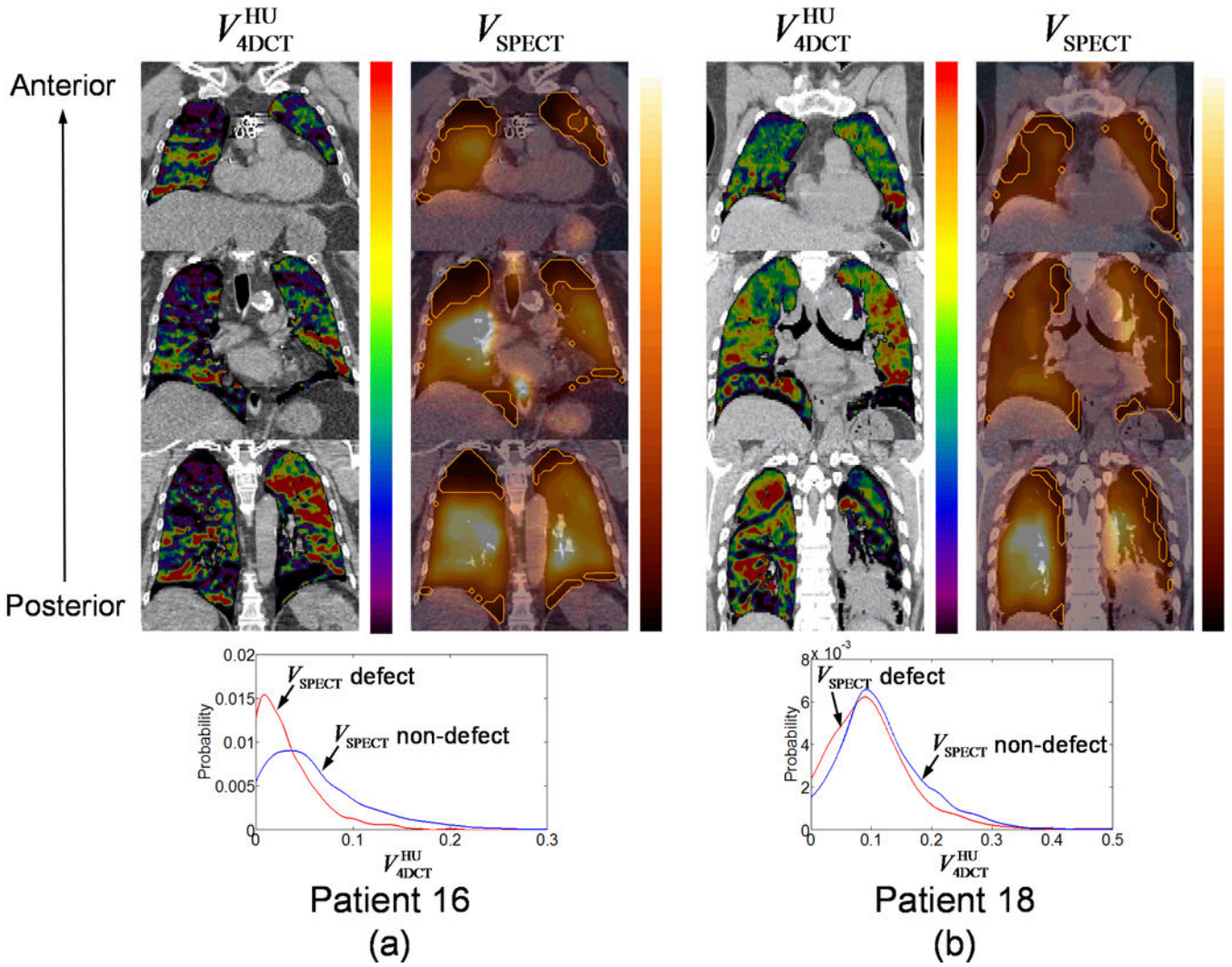


Figure 2. Comparison of V_{4DCT}^{HU} and V_{SPECT} for (a) patient 16, showing a large separation between the probability density functions of V_{4DCT}^{HU} in V_{SPECT} defect regions and non-defect regions, and (b) patient 18, showing a small separation. Orange outlines in V_{SPECT} denote defect regions. Both V_{4DCT}^{HU} and V_{SPECT} are shown with a scale from zero to the 90th percentile value.

Author Manuscript

Author Manuscript

Author Manuscript

Author Manuscript

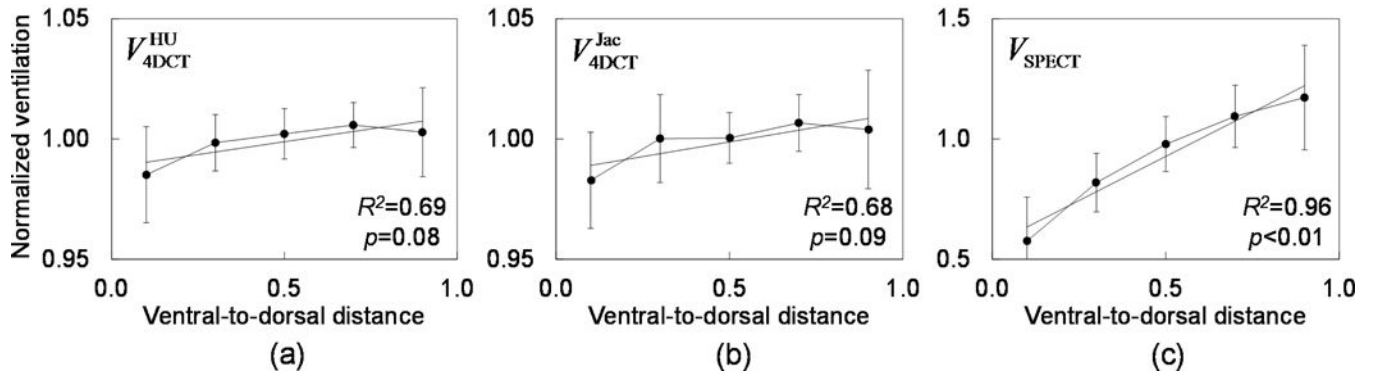


Figure 3.

Ventral-to-dorsal gradients of (a) V_{4DCT}^{HU} ($y = 0.02x + 0.99$), (b) V_{4DCT}^{Jac} ($y = 0.02x + 0.99$) and (c) V_{SPECT} ($y = 0.73x + 0.56$) for all the 16 patients for whom V_{SPECT} was available. Each data point (error bar) represents the mean value (standard deviation) of globally normalized ventilation in a coronal section-wise region of interest.

Table 1

Patient characteristics

Parameter	Value
Age (y)	67±12
Gender	
Male	15 (83.3)
Female	3 (16.7)
FEV ₁ (%pred) [*]	67±29
FVC (%pred) [†]	80±24
FEV ₁ /FVC (%) [‡]	69±24
DL _{CO} (%pred) [§]	79±25
Histology	
Lung cancer	14 (77.8)
Thoracic paraganglioma	1 (5.6)
Metastases to the lung	3 (16.6)
Clinical stage ^{**}	
I	3 (20.0)
II	2 (13.3)
III	6 (40.0)
IV	4 (26.7)
Lung volume (l) ^{††}	
Peak-exhale	3.6±1.7
Peak-inhale	4.2±1.8

Abbreviations: FEV₁ = forced expiratory volume in 1 s, FVC = forced vital capacity, DL_{CO} = diffusing capacity of the lung for carbon monoxide. Data are means ± standard deviations, or numbers with percentages in parentheses.

^{*} Available for 16 patients.

[†] Available for 14 patients.

[‡] Available for 15 patients.

[§] Available for 13 patients.

^{**} For 15 patients with primary lung cancer or thoracic paraganglioma.

^{††} Determined by the segmentation method for the 4D-CT images (see the Methods and Materials section).

Correlations between 4D-CT ventilation defect parameters and pulmonary function test (PFT) measurements

Table 2

PFT parameter	V_{4DCT}^{HU}		V_{4DCT}^{Jac}	
	25th percentile	Defect volume % defect volume	25th percentile	% defect volume
FEV ₁ (%pred) ⁷	0.45 (0.08)	-0.56 (0.03)	0.68 (<0.01)	-0.66 (<0.01)
FEV ₁ /FVC (%) ⁸	0.73 (<0.01)	-0.65 (<0.01)	0.73 (<0.01)	-0.64 (0.01)

Abbreviations: V_{4DCT}^{HU} = 4D-CT ventilation with Hounsfield unit 'HU' -change metric, V_{4DCT}^{Jac} = 4D-CT ventilation with Jacobian metric, FEV₁ = forced expiratory volume in 1 s, FVC = forced vital capacity.

Data are Pearson correlation coefficients (*R*). Values in parentheses are *p*-values.

⁷ Available for 16 patients.

⁸ Available for 15 patients.

Table 3

4D-CT ventilation in SPECT defect regions vs. in SPECT non-defect regions

Central airway depositions in V_{SPECT}	V_{4DCT}^{HU}		V_{4DCT}^{Iac}		<i>p</i> -value
	V_{SPECT} defect	V_{SPECT} non-defect	V_{SPECT} defect	V_{SPECT} non-defect	
None or non-severe (<i>n</i> =10)	0.056 (0.041)	0.093 (0.058)	0.071 (0.046)	0.088 (0.051)	0.03
Severe (<i>n</i> =6)	0.037 (0.028)	0.047 (0.027)	0.023 (0.007)	0.030 (0.007)	0.02
All (<i>n</i> =16)	0.049 (0.036)	0.076 (0.053)	0.053 (0.043)	0.067 (0.050)	<0.01

Abbreviations: V_{4DCT}^{HU} = 4D-CT ventilation with Hounsfield unit, HU; V_{4DCT}^{Iac} = 4D-CT ventilation with Jacobian metric, V_{SPECT} = SPECT ventilation. Data are mean V_{4DCT} values in V_{SPECT} defect regions and non-defect regions. Values in parentheses are standard deviations.